13th United States/North American Mine Ventilation Symposium, 2010 – Hardcastle & McKinnon (Eds.)

A new method to calculate permeability of gob for air leakage calculations and for improvements in methane control

C.Ö. Karacan
National Institute of Occupational Safety and Health (NIOSH), Office of Mine Safety and Health Research, Pittsburgh, Pennsylvania

ABSTRACT: The porosity and permeability of the caved zone in a longwall operation impact many ventilation and methane control related issues, such as air leakage into the gob, the onset of spontaneous combustion, methane and air flow patterns in the gob, and the interaction of gob gas ventholes with the mining environment. Despite their importance, the gob is typically inaccessible for performing direct measurements of porosity and permeability. Thus, there has always been debate on the likely values of porosity and permeability of the caved zone and how these values can be predicted. This study demonstrates a fractal approach that allows the calculation of porosity and permeability from the size distribution of broken rock material in the gob, which can be determined from image analyses. The fractal approach presented here constructs flow equations and fractal crushing equations for granular materials to predict porosity for a completely fragmented porous medium. The virtual fragmented fractal porous medium so generated is exposed to various uniaxial stresses to simulate gob compaction and porosity and permeability changes during this process.

1 Introduction

Longwall mining is an underground mining method that can maximize coal production in coal beds that contain few major geological discontinuities, like faults. Longwall coal mining causes large scale disturbances of the surrounding rock mass due to fracturing and caving of the mine roof behind the shields as the mine face advances. The gob is highly fragmented since the overlying rock layers fall into the mine void and are broken into irregular shapes of various sizes. The gob can contain high void ratios due to fragmented rock pieces and may provide high permeability flow paths for any fluid flowing from surrounding formations into the mining environment.

The porosity and permeability of the longwall gob can significantly affect methane and air flow patterns. Since methane is a major hazard in underground coal mining operations, extensive methane control techniques such as gob gas ventholes (GGV) are employed to supplement the existing mine ventilation system. Gob gas ventholes are drilled vertically into the overburden above longwall panels to capture the gas released by the fractured strata before it enters the mining environment. Most GGVs are drilled to within a short distance of the mined coalbed to stay out of the high-permeability gob so as not to draw excessive amounts of ventilation air along with the hazardous methane. In addition, the flow of mine air into the gob may increase the risk of spontaneous combustion. It has been shown that with an increase in gob permeability, airflow increases in the broken, coal-rich gob causing the onset temperature for spontaneous combustion to be reached more quickly (Yuan & Smith, 2008).

As mining progresses, the gob gradually consolidates sufficiently to support large loads resulting from the overburden weight (Pappas & Mark, 1993). Consolidation results in a reduction in the void ratio (porosity) and the associated permeability. Although reduced to some degree due to compaction, prevailing high permeability pathways in the gob still affect the leakage of ventilation airflow from the face into the gob, the flow of methane from surrounding sources into the gob and into the mine, and the performance of methane extraction GGVs. Thus, an understanding of compaction phenomena and the resultant reservoir properties of gob material is very important for developing adequate methane control strategies.

The properties of gobs and their influences on methane flow and control have been investigated through combined geomechanical and reservoir modeling (Esterhuizen & Karacan, 2005; Karacan *et al.*, 2007) and through history matching of GGV production. In these studies, geomechanical models were used to characterize the stress changes due to mining, which were converted to porosity and permeability data. Esterhuizen & Karacan (2007) presented the development of a new methodology to determine directional variations in gob permeability based on a model of caving and block rotation which considered the effect of block dimensions and fall height on porosity.

This work presents a fractal porous medium model to predict gob porosity and permeability for controlling methane flow and production from GGVs and to predict air leakage into the gob. For this approach, the particle size data for simulated gob material given by Pappas & Mark (1993) were used to calculate fragmentation fractal dimensions and particle size distributions before and after controlled loading tests. Fractal geometry concepts were used to construct porosity and flow equations for a completely fragmented porous medium through fragmentation, tortuosity and area fractal dimensions (Karacan & Halleck, 2003). The fragmented fractal porous

medium model was exposed to various uniaxial compressive stresses to simulate gob compaction and to predict porosity-permeability changes in the gob.

2 Laboratory Tests for Gob Material Simulation

In this paper, rock fragment size distribution data was taken from Pappas & Mark (1993) for model validation purposes. In order to better understand the behaviour of the gob and to provide numerical modellers with more accurate data for simulating longwall mining conditions, they conducted a laboratory study to estimate the gradation of actual gob material.

The first phase in the laboratory tests developed test materials with properties similar to those of actual gob material. The characteristics that were considered were the tensile and compressive rock strengths, rock density, surface roughness, rock shape, rock size, and size gradation. Most of these characteristics would be simulated by broken rock obtained from fresh roof falls. However, the rock size and gradation needed to be reduced to a laboratory scale by shifting the particle size distribution curve of the actual gob material determined from pictures taken from the headgate entries, where portions of the gob could be viewed. This shift was performed parallel to the horizontal axis of the particle-size curve until the desired maximum particle size of the laboratory sample was reached. The detailed procedure for this can be found in Pappas & Mark (1993). However, particle size affects the permeability of porous medium. Thus, the particle sizes used by Pappas & Mark (1993) were scaled up for use in the developed model to calculate permeability.

The rock types that were obtained to simulate gob were shale, weak sandstone and strong sandstone. In this paper, the size distributions obtained with maximum particle size of 5.1 cm (2.0 inches) for shale were used for modeling. Table 1 gives the test summary of simulated shale gob material.

Compressing a fragmented rock medium causes departures from the initial particle size distribution for both shale and sandstone material due to further crushing and fragmentation of the particles. This changes porosity and permeability. This will be discussed later in the rest of this paper.

Table 1 Summary of simulated materials (from Pappas and Mark, 1993) analyzed in this paper and their loading tests.

Rock	Max size cm	Max stress MPa	Initial por.	Por. @ 5.4 MPa	Por. @ max. stress
Shale	5.1	19.0	0.802	0.365	0.160

3 Model Development

3.1 Fractal Fragmentation and Formulation of a Deforming Fractal Porous Medium

Fragmentation may be considered as structural failure of a brittle material caused by multiple fractures of different lengths (Perfect, 1997). The disordered nature of pores and grains in fragmented porous medium suggests that the structure created by the fragmentation process shows scaling properties (Weiss, 2001). Fractal models not only can describe the scaling of mass and surface roughness of individual fragments, but also the fragment size distributions (Perfect & Kay, 1995).

The power law scaling of the number-particle size relation given by Turcotte (1986):

$$N(\omega > \Omega) = B_F \Omega^{-D_F} \tag{1}$$

where: N is the cumulative number of particles of size greater than a characteristic size Ω, the exponent D_F is referred to as the fragmentation fractal dimension and includes the information about the scale dependence of the number-size distribution of particles, and B_F is a coefficient related to number of particles of unit diameter.

In this study, the porous medium forming the gob was assumed to have pore sizes that can be considered as bundles of capillary tubes of different diameters as suggested by Yu & Cheng (2002). If the diameter of a capillary is assumed to be η and its tortuous length along the flow direction is Lt (η), then the tortuous length will be longer than its representative length L_O, which runs the shortest distance between two points. Following Wheatcraft & Tyler's (1988) expression and scaling approach for flow in a heterogeneous medium, there is a fractal scaling between the diameter and length of the capillaries (Yu & Chang, 2002):

$$L_t(\eta) = \eta^{1-D_T} L_o^{D_T} \tag{2}$$

In this equation, D_T is the tortuosity fractal dimension which can take values between 1 and 2. D_T represents the convoluteness of flow channels. When D_T is 1, the flow channels are straight. The tortuosity increases with increasing values of D_T. In the limiting case of D_T =2, we have a highly tortuous line that fills a plane (Wheatcraft & Tyler, 1988). However, Wheatcraft & Tyler (1988) reported that D_T values more than 1.5 do not have any physical significance.

For the bundle of capillaries or flow channels, the number of channels with size η is also important. Since channels in a porous medium are analogous to the islands in a sea or spots on surfaces, the cumulative size distribution of pores can be written as:

$$N(L \geq \eta) = \left(\frac{\eta_{\max}}{\eta} \right)^{D_P} \tag{3}$$

In this equation, N is the number of pores whose sizes (η) are greater than a characteristic size, L and η_{max} is the maximum pore size. Equation 3 can be differentiated to give:

$$-dN = D_P \eta_{\max}^{D_P} \eta^{-(D_P+1)} d(\eta) \tag{4}$$

In Equation 4, D_P is the pore area fractal dimension ($1< D_P <2$). A D_P value of 2 represents a regular pore area and the irregularity increases for D_P <2. These equations describe the scaling relationship of cumulative pore populations. The total number of pores from the smallest diameter, η_{min}, to the largest diameter, η_{max}, thus can be obtained from the Equations 3 and 4 as:

$$N_t(L \geq \eta_{\min}) = \left(\frac{\eta_{\max}}{\eta_{\min}}\right)^{D_P} \tag{5}$$

Dividing Equation 4 by Equation 5 obtains an expression for the probability density function:

$$-\frac{dN}{N_t} = D_P \eta_{\min}^{D_P} \eta^{-(D_P+1)} d(\eta) = f(\eta) d(\eta) \tag{6}$$

where

$$f(\eta) = D_P \eta_{min}^{D_P} \eta^{-(D_P+1)} \tag{7}$$

The equations above can be used as a model of a capillary tube bundle of any shape.

In order to characterize a pressure-driven, steady state flow of a fluid through long, straight, and rigid channels of any constant cross-sectional shape, with no-slip boundary conditions, the Hagen-Poiseuille (H-P) flow equation can be used. H-P equation for a circular area:

$$Q_i = \frac{\pi \Delta P \eta^c}{16 \alpha \mu L_t} \tag{8}$$

where η is the hydraulic diameter and L_t is the total length of the channel. In circular pipes, α=8 and the flow-channel diameter exponent "c" of the equivalent channel diameter is 4. For some known shapes such as rectangle, the shape correction factor (α) is given by Mortensen *et al* (2005):

$$\alpha = \frac{\pi^3 \gamma^2}{8} \left(\sum_{n=1,3,5\ldots}^{\infty} \frac{\gamma}{\pi n^4} - \frac{2}{\pi^5 n^5} \tanh\left(\frac{n\pi\gamma}{2}\right) \right)^{-1} \tag{9}$$

where γ is the width-to-height (w/h) ratio of the rectangular channel. Tanh(x) can be approximated to 1 if x is very large which can be satisfied if γ is very large (slit shaped channels for example). In this case Equation 9 becomes;

$$\alpha = \frac{12\pi^5 \gamma^2}{\pi^5 \gamma - 186\zeta(5)} \tag{10}$$

where $\zeta(5)$ results from truncating the summation after 5th iteration in Equation 9.

In this paper, the average diameter exponent from Arya *et al.*'s work (1981) will be used in the H-P equation (Equation 8) to describe flow in single channels (3.531). The variable "α" (Equations 9 & 10) will be retained in the equation to run parametric analyses related to channel shape. Thus, H-P equation from a single channel becomes:

$$Q_i(\eta) = \frac{\pi}{16} \frac{\Delta P}{L_t(\eta)\alpha} \frac{\eta^{3.531}}{\mu} \tag{11}$$

If the total flow rate is calculated for each channel by integrating between the minimum and maximum sizes over the entire range of pore sizes, the total flow rate is obtained as;

$$Q_T = -\int_{\eta_{\min}}^{\eta_{\max}} Q_i(\eta)\, dN(\eta) = \frac{\pi}{16} \frac{\Delta P}{\mu} \frac{L_o^{-D_T}}{\alpha} \frac{D_P}{2.531 + D_T - D_P} \times \eta_{\max}^{2.531+D_T} \left[1 - \left(\frac{\eta_{\min}}{\eta_{\max}} \right)^{2.531+D_T-D_P} \right] \tag{12}$$

For the special case of circular channels, this equation is:

$$\boldsymbol{Q_T = \frac{\pi}{128} \frac{\Delta P L_o^{-D_T}}{\mu} \frac{D_P}{3 + D_T - D_P} \times \eta_{\max}^{3+D_T} \left[1 - \left(\frac{\eta_{\min}}{\eta_{\max}} \right)^{3+D_T-D_P} \right]} \tag{13}$$

Equations 12-13 honour the properties of H-P equation where the streamlines are formed by individual particle sizes that create tortuous pores of a particular dimension and shape and those they do not really mix. Combining Equations 12 and 13 with Darcy's Law ($Q_T = \frac{kA_T \Delta P}{\mu L_o}$), where k is the permeability and A_T is the total area to flow, yields the definition of permeability for a porous medium composed of tortuous channels of varying diameters and shapes:

$$k = \frac{\pi}{16 A_T} \frac{L_o^{1-D_T}}{\alpha} \frac{D_P}{2.531 + D_T - D_P} \eta_{\max}^{2.531+D_T} \times \left[1 - \left(\frac{\eta_{\min}}{\eta_{\max}} \right)^{2.531+D_T-D_P} \right] \tag{14}$$

For circular channels;

$$k = \frac{\pi}{128}\frac{L_o^{1-D_T}}{A_T}\frac{D_P}{3+D_T-D_P}\eta_{\max}^{3+D_T}\left[1-\left(\frac{\eta_{\min}}{\eta_{\max}}\right)^{3+D_T-Dp}\right] \quad (15)$$

In these equations, total area of flow (A_T) is the combination of areas for both pores and the rock surface exposed to the flow. Since the gob material in the caved zone is highly fragmented and the total channel area is the same as the effective porosity where the flow occurs, total channel area (A_P) is used for A_T. In order to determine the value of A_P, the areas of individual flow channels can be summed mathematically to give (Karacan, 2009):

$$A_T = A_p = \sum_{i=1}^{s}\left(\frac{\pi\Omega_i^2}{6}\phi_i N_i^{1-D_T}\right) \quad (16)$$

as a combination of virtual pore-size fractions (Rieu & Sposito, 1991) for total porosity and formed by broad range of pore sizes. Since the pores are assumed to be formed in a packing arrangement of the grains and the relation of η_i (mean pore diameter in the i^{th} virtual pore size fraction) with Ω_i ,then the number of pore-size classes can assumed to be equal to the number of particle size classes ("s" in Equation 16). Total porosity in terms of particle sizes is defined as:

$$\phi_T = 1-\left(\frac{\Omega_{\min}}{\Omega_{\max}}\right)^{3-D_F} \quad (17)$$

where D_F is the fragmentation fractal dimension that can be determined from the slope of the best linear fit to the number-size relation given in Equation 1.

In the caved zone of longwall gobs, the degree of compaction is a function of initial porosity and strength of the rock fragments. The initial porosity varies with the shape of rock fragments, their sizes and size distribution (Yavuz, 2004). He notes that the initial compaction of caved material will be larger during the initial loading (compression) stage. As compression increases, the broken material will stiffen due to the densely compacted material and a reduction in porosity in the caved zone will result by further crushing or fragmentation of the initial rock pieces. Crushing is accompanied by changes in particle size distribution. The crushing strength of a particle is a function of its size and its co-ordination number (number of contacts with neighbours). In the case of a large population of granular materials subjected to the above processes, the change in compaction is important for evaluating porosity.

Using the principles of grain crushing and a particle-size distribution modeled as a self-similar pattern, the plastic reduction in porosity with a one-dimensional applied stress increment is given by (McDowell *et al.*, 1996):

$$d\phi_T = -\beta f^{\frac{(1-D_F)}{2}}\frac{\varepsilon}{(1-\kappa)\overline{\sigma}\Omega_{\max}}(2-D_F) \times m\sigma_0^{\frac{m(1-D_F)}{2}}\overline{\sigma}^{\frac{m(D_F-1)}{2}-1}d\overline{\sigma} \quad (18)$$

In this equation D_F is the fragmentation fractal dimension defined by Equation 1, ε is the surface energy in linear-elastic fracture mechanics (Griffith, 1920), m is the Weibull modulus based on the observations that particle-survival probability follows a Weibull distribution, σ_0 is the tensile strength of the grains, $\overline{\sigma}$ is the applied macroscopic stress and f is fracturing probability term (McDowell *et al*., 1996). This equation can be written in a more compact form by separating it into the plastic compressibility index (Λ) and stress increment ($d\overline{\sigma}$) terms:

$$d\phi_T = -\Lambda\overline{\sigma}^{\frac{m(D_F-1)}{2}-2}d\overline{\sigma} \quad (19)$$

where Λ is defined as:

$$\Lambda = \beta f^{\frac{(1-D_F)}{2}}\frac{\varepsilon}{(1-\kappa)\overline{\sigma}\Omega_{\max}}(2-D_F)m\sigma_0^{\frac{m(1-D_F)}{2}} \quad (20)$$

Equation 19 can be integrated, assuming Λ is constant at each stress level, between two successive stress increments (i to i+1) to obtain (Karacan, 2009):

$$\phi_{T_{i+1}} - \phi_{T_i} = -\Lambda\left[\frac{\overline{\sigma}_{i+1}^{\frac{m(D_F-1)}{2}-1}}{\frac{m(D_F-1)}{2}-1} - \frac{\overline{\sigma}_i^{\frac{m(D_F-1)}{2}-1}}{\frac{m(D_F-1)}{2}-1}\right] \quad (21)$$

In order to solve Equations 19-21, the plastic compressibility index (Λ) should be defined by either substituting typical values of physical parameters in Equation 20 or by using a typical value of 0.1 for sands and clays (McDowell *et al.*, 1996).

3.2 How to Determine Model Parameters

In effect, Equations 19-21 evaluate the change in porosity as a function of increasing vertical stress and fragmentation fractal dimension. In each iteration, or incremental vertical stress, the new porosity replaces the porosity term (Ø) in Equation 16 to modify total flow area (A_T). Finally, the updated flow area is inserted into Equation 14, for rectangular channel openings or Equation 15 for cylindrical channels, to estimate the permeability at a particular stress and fragmentation level (Karacan, 2009).

The general solution procedure stated above requires determination of these parameters: representative length "L_o", maximum and minimum particle dimensions "Ω_{min} and Ω_{max}" in the range(s) that shows fractal behaviour, Weibull modulus "m", pore, tortuosity and fragmentation fractal dimensions "D_P, D_T and D_F" respectively, virtual

pore size classes "s", minimum and maximum pore (channel) diameters "η_{min} and η_{max}".

Weibull modulus (m) is a measure of the variability in strength of the material. For chalk, brick, stone and cement, m is between 1 and 5 (McDowell *et al.*, 1996). Engineering ceramics, for instance, have values for m of about 10 due to much less variation in strength compared to natural rocks or compared to composite materials with relatively high inter- and intra-particle porosities and flaws. Thus, a low m-value around 2 should be expected for natural materials.

Representative length (L_o) is defined as the shortest distance between two points where there is a pressure differential that drives the flow. These two points may be on either side of the measurement interval within the gob or from a point in the gob to the gateroads. Therefore, the representative lengths change based on the location of the evaluation points in the gob.

Fragmentation fractal dimension (D_F) defined by Turcotte (1986) showed that particle sizes of geologic materials exhibit fractal behaviour as shown in Equation 1. The cumulative number versus particle size relation (Figure 1) that is used to determine D_F can also be used to find the maximum and minimum particle size. Maximum and minimum particle diameters (Ω_{min} and Ω_{max}) are approximately the cut-off limits of deviation from linearity in the number-size relation. The fragmentation fractal dimensions and maximum and minimum particle sizes before and after loading tests are listed in Table 2.

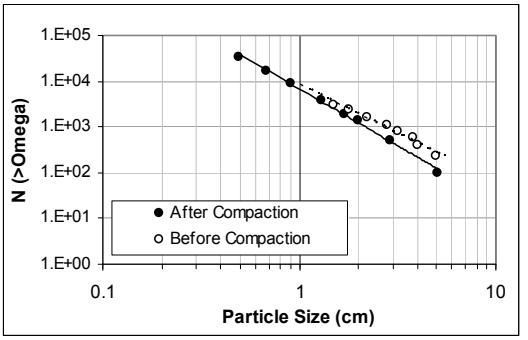

Figure 1 Log-log plots for number-particle size data (Equation 1) for shale test before and after loading. D_F's for this test - before compaction and after compaction are 2.19 and 2.89, respectively.

The number of virtual pore size classes "s" is equal to the number of different particle size fractions that are within the cut-off limits of the data set where fractal scaling is observed. Since a linear trend is observed between all particle size classes, the number of particle size classes used will be the same as the virtual pore size fractions (Table 2).

Fractal dimension of the one-dimensional trace of pore channel (D_T), or tortuosity fractal dimension, describes how the pores are convoluted in relation to Lo. However, it is not always easy to determine the tortuosity of a channel to find its fractal dimension. In this study, the "slit-island" theorem of Mandelbrot *et al*. (1994) was used to determine D_T, since there is really no practical means of measuring this parameter. This approach has been used in the literature (Sammis & Steacy, 1995) to estimate the fractal dimension of lower order geometries.

In order to apply the slit-island theorem to estimate the tortuosity fractal dimension (D_T) in the crushed material, the fractal increment values reported by various researchers on different type of soil and porous rocks were evaluated. Jacquin & Adler (1988) observed fractal increments of 0.23 in pore structures of dolomitic limestone. Tyler & Wheatcraft (1989) reported fractal increments between 0.14 and 0.43, with an average of 0.23 when obtained from soil particle size data. Karacan & Halleck (2003) determined that an average D_T increment of 0.29 for incompletely fragmented porous media using shock waves. These increments can be used to calculate D_T values of 1.23 and 1.29 from these references for highly compacted and incompletely fragmented porous media, respectively. The average of these two values (1.26) will be taken as the representative value for the compacted gob. For the initial gob material, 1.10 will be used as the average of D_T. This value is based on the averages calculated by Wheatcraft & Tyler (1988) as 1.08 using Monte-Carlo simulations, values reported by Yu & Cheng (2002), and Yu & Liu (2004) for pores in 52% porosity medium between 1.10-1.12. These values have physical sense since compaction or incomplete fragmentation compared to complete fragmentation increases the tortuosity of pore channels.

Table 2 Results of D_F, D_T, D_P and maximum (Ω_{max}) and minimum (Ω_{min}) particle sizes (up-scaled) determined before and after loading tests using number-size relationship

Before Loading			
s	**D_F**	**Ω_{min} (cm)**	**Ω_{max} (cm)**
9	2.19	15	51
Before Loading			
D_T (straight)	**D_T (tortuous)**	**D_P (uniform)**	**D_P (irregular)**
1	1.10	2	1.19

After Loading			
s	**D_F**	**Ω_{min} (cm)**	**Ω_{max} (cm)**
10	2.89	5	51
After Loading			
D_T (straight)	**D_T (tortuous)**	**D_P (uniform)**	**D_P (irregular)**
1	1.26	2	1.89

If the pore area represents a smooth object (circle, square, triangle etc.) covering the whole area, then D_P can be taken as 2. If the pores are irregular in shape and distribution, then their area-fractal dimension will be less

than 2 (Ahmed & Dryzmala, 2005). In case of irregular pore shapes and distributions, slit-island theorem can be used by employing the D_F values (Table 2) obtained in this study. Since particle size distribution is a 3-dimensional entity (Tyler & Wheatcraft, 1989), its Euclidean dimension is 3. Then, the calculated increments (D_F-3) are added to the Euclidean dimension for area to obtain D_P (Table 2).

Tortuosity (D_T) and pore-area (D_P) fractal dimensions for straight and regular pores as well as the values determined using the above approaches for the convoluted and irregular pores are given in Table 2. These values will be used in model calculations later in this paper.

In order to calculate porosity and permeability using actual gob-material sizes and their distributions, the gradation curves of laboratory-simulated gob material were up-scaled by 10 times to their original sizes. Up-scaling, in effect, changes particle sizes and eventually the channel sizes that will be calculated based on particle size. However, as long as the gradation curve is held constant, up-scaling does not change the fragmentation fractal dimensions since this will not change the slope. Thus, the fractal dimensions reported in Table 2 will still be valid.

The size of the grains in a fragmented porous media will directly affect the pore flow area and pore diameters forming between the grains. In order to calculate permeability under increasing loading, up-scaled grain sizes will be used in area- and pore-size calculations. In order to incorporate the effect of loading on permeability, a fractal crushing model for porosity will be integrated into calculations.

Equation 16 is used to calculate the total flow area in the fragmented gob material. This equation can alternatively be represented with an integral:

$$\frac{\pi}{3}\int_{\Omega_{min}}^{\Omega_{max}} \Omega\ \phi\ N^{1-D_T}\, d\Omega \qquad (22)$$

In this integral, maximum and minimum particle sizes are the up-scaled values and the number (N) is a function of grain size. In order to find this function, the numbers of up-scaled particles for each up-scaled size were plotted (Figure 2). By up-scaling the material mass (assuming density stays constant) by 1000 times due to a 10 fold increase in particle diameter, the functional relationship given in Equation 23. Figure 2 shows that as diameters increase, the number of particles decreases, as expected. More importantly, the figure shows that the data can be successfully represented by power functions.

In Equation 16, Ø-values are the partial porosities for each infinitesimal size interval. Integration between Ω_{min} and Ω_{max} will result in the total fractal porosity ($Ø_T$), which will not be dependent on Ω. With these treatments, the fractal flow area (Equation 16) becomes:

$$\frac{\pi}{3}\phi_T\int_{\Omega_{min}}^{\Omega_{max}} \left(10326\Omega^{-1.74}\right)^{1-D_T}\Omega\, d\Omega \qquad (23)$$

After rearrangement, the integral shown below is obtained:

$$\frac{10326^{1-D_T}\,\pi}{3}\phi_T\int_{\Omega_{min}}^{\Omega_{max}} \Omega^{-0.74+1.74D_T}\, d\Omega \qquad (24)$$

Solving the integral gives the fractal pore area for initial gob material as:

$$A_T = A_P = \frac{10326^{1-D_T}\,\pi}{3}\phi_T\left[\frac{\Omega_{max}^{\,0.26+1.74D_T}}{1.74D_T+0.26} - \frac{\Omega_{min}^{\,0.26+1.74D_T}}{1.74D_T+0.26}\right] \qquad (25)$$

This equation can directly be used in Equations 14 or 15 for "area"once the fractal bounds of particle sizes and the size of the flow channels are determined. In Equation 25, $Ø_T$ is the porosity which changes as uniaxial stress progressively increases according to Equations 19-21 (Karacan, 2009).

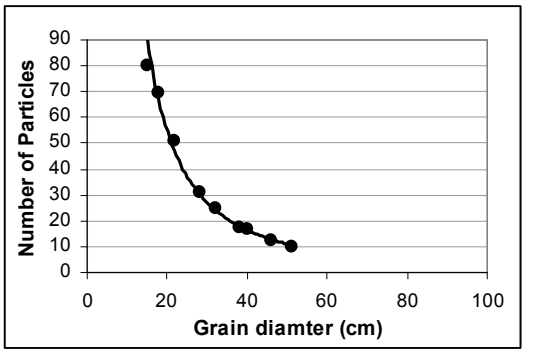

Figure 2 Number-size distributions for the up-scaled diameters for the initial gob material.

In order to determine maximum and minimum channel sizes, Equation 26 given below is used.

$$\eta_i = \Omega_i\left(\frac{2}{3}\phi_i\, N_i^{1-D_T}\right)^{1/2} \qquad (26)$$

This equation gives the sizes of flow channels in each partial volume of a fractal porous medium. In this equation, the number term (N) is replaced by its functional form given in the integrand in parenthesis of Equation 23. The partial porosity term in the equation is, on the other hand, the amount of porosity in that partial volume (Rieu & Sposito, 1991). In order to obtain partial porosity, the total porosity at a particular loading stage can be divided by the "virtual pore size fractions" or the number of particle size classes "s" given in Table 2. This value was around 9-10 in this study as tabulated in Table 2. With these additions, the maximum and minimum channel diameters (η_{max} and η_{min}) as a function of Ω can be calculated. These relations are given in Table 3.

Table 3 Minimum and maximum sizes (η_{min} and η_{max}) of tortuous flow channels as a function of particle size. Particle diameters to be used are the up-scaled values. The units of both particle sizes and the resulting channel sizes are in cm.

η_{max}
$0.82\sqrt{\frac{\phi_T}{s}\left(10236^{1-D_T}\right)\Omega_{\max}^{0.26+1.74D_T}}$
η_{min}
$0.82\sqrt{\frac{\phi_T}{s}\left(10236^{1-D_T}\right)\Omega_{\min}^{0.26+1.74D_T}}$

4 Model Application to Predict Gob Porosity and Permeability under Loading

4.1 Porosity of Initial and Compacted Gob Material

In order to compare the initial porosities given by the experiment at 0.0 MPa load (Table 1) with the initial porosities calculated using particle size distribution and fractal model equations, Equation 17 was used first. This equation requires the upper and lower bounds (in terms of particle size) of distribution across which a fractal scaling is observed and the calculated fragmentation fractal dimension. Since the size distributions given in Figure 1 reveal reasonably good linear relations for the initial gob material, the upper- and lower-size limits were selected to capture the whole particle-size range in each test (Table 2). In addition, the D_F's given in Table 2 were used for the same cases.

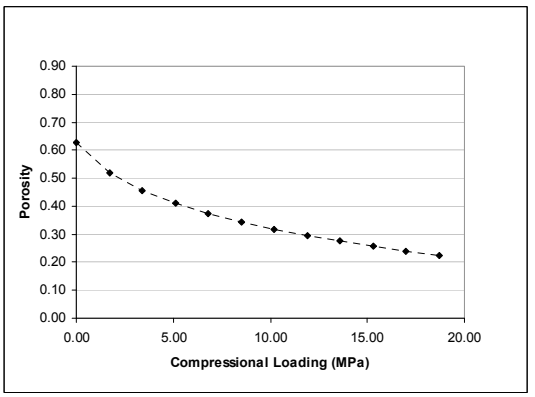

Figure 3 Porosity predicted for compacting gob materials using Equations 17-21.

The porosity values obtained using Equation 17 and the values determined in the laboratory before loading are 0.63 and 0.8, respectively. Before calculating the porosities using particle size distributions and the theory described in previous sections, porosities that should be experienced in the gob were calculated using the experimental stress-strain curve (Pappas & Mark, 1993) and the initial porosity determined from Equation 17 (0.63). The results of this calculation are shown in Figure 3.

The porosity evaluation during uniaxial compression of simulated gob material shows that at earlier loadings, the material could be compressed more when compared to later stages. At around a stress level of 19 MPa (2750 psi), the predicted final porosity of the material was about 20-22%. A difference of 4-5% between the values given in Figure 3 and the values in Table 1 can be considered close for this analysis. As an inner check point, the porosity values reported in Table for 5.4 MPa (800 psi) were compared with the corresponding data shown in Figure 3. These values are also within 2-3% of each other.

As the longwall face advances during mining and the overburden starts settling on the caved material, the initially caved gob material is subjected to progressively increasing stresses. These stresses decrease the initially observed high porosities by crushing the gob material into smaller pieces as shown in the previous sections (Figure 3).

The porosity of simulated gob material after laboratory loading test was calculated by using the particle size distributions data after the test (Figure 1) and the fractal model given in Equation 17. In summary, a similar procedure that was followed to calculate initial porosities was applied. The porosities were calculated using the fragmentation fractal dimensions given in Table 2 within the linear range of particle size data (Figure 1) where fractal behaviour is observed. For these calculations, the lower bound of the particle diameter after loading was determined as 5 cm (for up-scaled diameters). In this calculation, a porosity value of 0.23 was predicted, compared to 0.16 that was obtained during laboratory tests. Again, this difference between predictions and reported/calculated values can be regarded as acceptable predictions for practical purposes.

The porosity calculated using fractal methods and the number-size relations discussed so far and their comparison with laboratory measured or calculated data shows that the gob material forms a fractal porous medium. The porosity of this medium, before or after being subjected to a vertical stress, can be calculated within an acceptable error using number-size distribution data available for the fragmented gob material. The evolution of the porosity during the entire loading period can also be estimated by using Equations 17-21, as presented in Figure 3. This suggests that the fractal crushing equation can be used to predict evolving porosities in a gob as a result of compression. One can use the initial number-size distribution of a granular media and its fragmentation fractal dimension to calculate changing porosities as stress is progressively increased.

4.2 Calculation of Permeability of Initial and Compacted Gob Material

In order to calculate gob permeability, Equations 14 or 15 can be used depending on the expected shape of the flow channels. Certainly, this is a hard judgment to make for a

complex fragmented medium. However, in any case, in this study the channels were taken as rectangular shaped pores, channels, and even as slit-like rectangular geometries. Mathematically, this transition in the shape can be created by changing the aspect ratio (Equations 9-10) between the two-axes of the rectangular geometry for use in the H-P type flow and permeability prediction.

In order to calculate permeability of a gob composed of broken rocks and rectangular flow channels, Equation 14 was used. In this equation, total pore area for flow was calculated using Equation 25 and the flow channel sizes were taken as in Table 3. As it can be noticed, the flow area is a function of particle size and tortuosity and area fractal dimensions (D_T and D_P). Flow channel sizes are also a function of D_T. In the permeability calculations, the D_T=1.26 was used as tortuosity of the rectangular channels, whose areas were irregular (D_P=1.19). The up-scaled maximum and minimum rock sizes (Ω_{max} and Ω_{min}) for initial gob material were based on Table 2.

Table 4 shows the aspect ratios used for the rectangular channels and the calculated shape factors (Equation 9). As this table indicates as the aspect ratio increases, i.e. as the rectangular opening becomes more of a slit-like structure, the shape factor increases. Also, since shape factor (α) is in the denominator of Equation 14, the value of permeability is expected to decrease. This is a situation that is expected in reality too.

Table 4 Aspect ratios used and the calculated shape factors for rectangular flow channels.

Aspect Ratio	Shape Factor
10	149.32
20	266.13
100	1224.04
250	3023.75
750	9023.63
5000	60023.57

Figures 4 and 5 show the predicted permeability of rectangular channels of various aspect ratios in gob as a function of uniaxial compressive load. Both figures show that the permeability is higher initially and decreases as a result of crushing and compaction during loading. The predicted permeabilities are changing from 0.00011 cm^2 (11×10^3 Darcy) for a gob initially composed of bigger rocks forming irregular, meandering tortuous channels of rectangular shape and 10:1 aspect ratio to 0.00004 cm^2 (4×10^3 Darcy) for the same gob under compressional loading. When the initial aspect ratio is 20:1, the initial permeability is around 0.00006 cm^2 (6×10^3 Darcy), which decreases to 0.000025 cm^2 (2.5×10^3 Darcy) when the gob is compressed (Figure 4). As it can be seen from Figures 4 & 5, as the aspect ratio increases the initial and final permeabilities decrease for each of the six cases modeled for this paper.

The obvious question, of course, is how these permeabilities compare with the measurements. Unfortunately, there are not any field measurements of

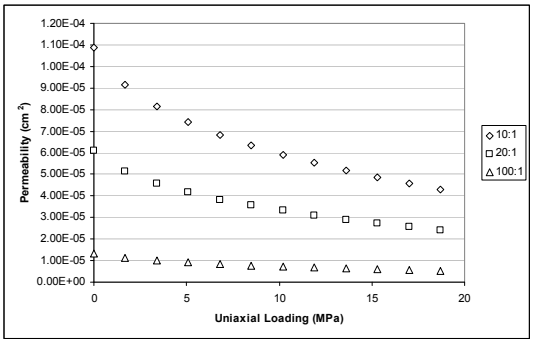

Figure 4 Calculated permeability change for a shale-rich gob, where porous space for gas migration is formed with irregular rectangular channels of geometrical aspect ratios of 10:1, 20:1, 100:1.

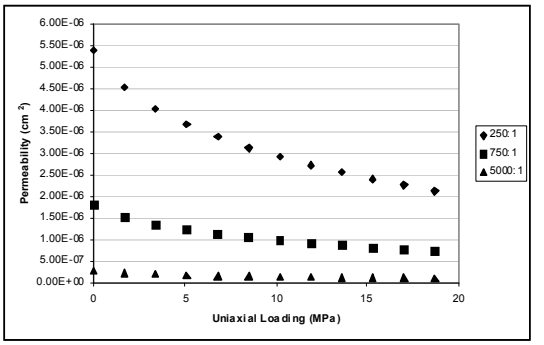

Figure 5 Calculated permeability change for a shale-rich gob, where porous space for gas migration is formed with irregular rectangular channels of geometrical aspect ratios of 250:1, 750:1, 5000:1.

permeability of gobs due to their inaccessibility for performing direct measurements. However, there are some reported values calculated based on volumetric strains and geomechanical calculations. For instance, Brunner (1985) used gob permeability values in ventilation network models as 1×10^{-7} m^2 to 1×10^{-5} m^2 (1×10^5 to 1×10^7 Darcy). Ren *et al.* (1997) estimated the permeability in the gob to be on the order of 1×10^{-10} m^2 (1×10^2 Darcy) in the compacted region. Wendt & Balusu (2002) used maximum values around 1×10^{-9} m^2 (1×10^3 Darcy). Whittles *et al.* (2006) reported calculated values in the range of 5×10^{-7} m^2 (5×10^5 Darcy) to 1×10^{-8} m^2 (1×10^4 Darcy) for a gob. Esterhuizen & Karacan (2007) reported calculated values of 1×10^{-9} m^2 (1×10^3 Darcy). The differences in reported permeabilities may be related to different coal-seam geologies, different panel layouts and to differences in caving characteristics. Nevertheless, it should be noted that all these reported values are within similar orders of magnitude and close to the permeability values calculated by the fractal flow models presented in this study. Thus, the fractal-fragmentation and fractal-crushing driven methodologies and the flow models presented in these

analyses can predict permeabilities close to the values reported in other studies.

5 Summary and Conclusions

This study developed a predictive approach using the principles of scaling and fractal porous medium combined with fluid flow. The fractal approach constructed flow equations and fractal crushing equations for granular materials to predict porosity and permeability for a completely fragmented porous medium. The virtual fragmented fractal porous medium so generated was exposed to various uniaxial stresses to simulate gob compaction and porosity and permeability changes during this process for various flow channel complexities and irregularities.

Particle size distributions of gob material determined from digital pictures or from simulated tests can be used to find the fragmentation fractal dimension of gob material based on a number-size relationship, which then can be used to find porosity. Fluid flow in a fractal porous media, on the other hand, can be described using fractal scaling between pore and grain sizes. These information can be used in the Hagen-Poiseuille (H-P) equation to describe flow rate, which then can be integrated with the Darcy equation to describe permeability of a fractal porous media in terms of textural and fractal properties. Moreover, fractal crushing of granular materials can be used in the definition of flow area to simulate compaction of a gob. In this study, the porosities predicted using a fractal crushing model were found to be in good agreement with the porosity values calculated using stress-strain data and particle size data.

Geometrically, circular and smooth channels should give the highest permeability. This study was conducted on rectangular-shaped geometries as a more realistic approach to channel shapes in the gob. Based on this approach, it was shown that as the irregularity and aspect ratio of the channels increase, permeabilities decrease as expected.

This paper demonstrated a new approach to calculate porosity and permeability of gob. Using the approach developed in this paper, it is possible to make predictions of gob porosity and permeability. This will lead to predictions regarding the flow amount and flow patterns in the gob. The ability of improving predictions in the flow amounts and flow patterns in the gob using this simple technique will lead to performing leakage calculations and methane control projections. However, one should exercise caution in treating the data from either digital images or from particle size experiments as the technique is closely related to geometrical and scaling parameters. Therefore, results can be sensitive to errors in data analyses, which can lead to spurious porosity and permeability values.

Nomenclature

A_G	area of grains
A_P	area of pores
A_T	total area
D_F	fragmentation fractal dimension
D_P	pore area fractal dimension
D_T	tortousity fractal dimension
f	fracturing probability term
h	thickness of the analysis location
k	permeability
L_t	tortuous length
L_o	representative length
s	number of virtual pore size fractions
N_i	number of particles in the i^{th} size class
ΔP	differential pressure
m	Weibull modulus
Q	total flow rate
V	volume of porous medium

Symbols

α	shape factor in H-P equation
η	pore diameter
η_i	pore diameter of the i^{th} size class
ϕ	porosity of fragmented porous medium
ϕ_i	porosity in partial volume in fractal porous media
ϕ_T	total porosity
μ	viscosity
Ω_i	particle diameter of the i^{th} size class
$\overline{\Omega}$	average particle diameter
Π	hydraulic resistance
Ψ	arbitrary cross sectional area
Λ	plastic compressibility index
$v(x, y)$	fluid velocity perpendicular to x-y plane
ε	surface energy in linear-elastic fracture mechanics
σ_0	tensile strength of the grains
$\overline{\sigma}$	applied macroscopic stress

Permeability conversion factor

1 Darcy 10^{-12} m^2 = 10^{-8} cm^2

References

Ahmed, A.M.H. & Drzymala, J. (2005). Two-dimensional fractal linearization of distributed curves. Physicochemical Problems of Mineral Processing 39, 129-139.

Arya, L.M., Paris, J.F., (1981). A physicoemprical model to predict the soil moisture characteristics from particle-size distribution and bulk density data. Soil. Sci. Soc. Am. Journal, 45, 1023-1030.

Brunner, D.J. (1985). Ventilation models for longwall leakage simulation. Proc. 2nd US Mine Ventilation Symposium, 23-25 September, Reno, NV.

Esterhuizen, G.S. & Karacan, C.Ö. (2005). Development of numerical models to investigate permeability changes and gas emission around longwall mining panels. The AlaskaRocks 2005, 40th US Symposium on Rock Mechanics, Anchorage, Alaska, 25-26 June.

Esterhuizen G.S. & Karacan C.Ö. (2007). A methodology for determining gob permeability distributions and its application to reservoir modeling of coal mine longwalls. 2007 SME Annual Meeting, Denver, CO.

Griffith, A.A. (1920). The phenomena of rupture and flow in solids. Philos. Trans. R. Society of London A221, 163-198.

Jacquin, C. G. & Adler, P. M. (1988). Fractal porous media II: geometry of porous geologic structures. Transport in Porous Media, 2, 571-596.

Karacan, C.Ö. (2009). Prediction of porosity and permeability of caved zone in longwall gobs. Transport in Porous Media (in press).

Karacan, C.Ö. & Halleck, P.M. (2003). A fractal model for predicting permeability around perforation tunnels using size distribution of fragmented grains. J. Petroleum Sci. and Eng. 40, 159-176.

Karacan, C.Ö., Esterhuizen, G.S., Schatzel, S.J. & Diamond, W.P. (2007).Reservoir simulation-based modeling for characterizing longwall methane emissions and gob gas venthole production. International Journal of Coal Geology 71 (2-3), 225-245.

Mandelbrot, B.B., Passaja, D.E. & Paulley, A.J. (1994). Fractal character of fracture surfaces of metals. Nature, 21, 308.

McDowell, G.R., Bolton, M.D. & Robertson, D. (1996). The fractal crushing of granular materials. Journal of the Mechanics and Physics of Solids 44, 2079-2101.

Mortensen, N.A., Okkels, F. & Bruss, H. (2005). Reexamination of Hagen-Poiseuille flow: Shape dependence of the hydraulic resistance in microchannels. Physical Review E 71, 057301, 1-4.

Pappas, D.M., & Mark, C. (1993). Behavior of simulated longwall gob material. Report of Investigations RI No. 9458, US Dept. of Interior, US Bureau of Mines.

Perfect, E. & Kay, B.D. (1995). Applications of fractals in soil and tillage research: a review. Soil Tillage Res. 36, 1-20.

Perfect, E. (1997). Fractal models for the fragmentation of rocks and soils: a review. Engineering Geology, 48, 185-198.

Ren, T.X., Edwards, J.S. & Josefowicz, R.R. (1997). CFD modeling of methane flow around longwall coal faces. Proc 6th International Mine Ventilation Congress, 17-22 May, Pittsburgh, PA.

Rieu M. & Sposito, G. (1991). Fractal fragmentation, soil porosity and soil water properties: theory, Soil. Sci. Soc. Am. J., 55, 1231-1238.

Sammis, C.G. & Steacy, S.J. (1995). Fractal fragmentation in crustal shear zones. In: Fractals in the Earth Sciences. Barton C., La Pointe, P.R. (Eds.), Pleanum Publishing Co., New York, NY. 265 pp.

Turcotte, D.L. (1986). Fractals and fragmentation. J. Geophysical Res. 91, 1921-1926.

Weiss, J. (2001). Fracture and fragmentation of ice: a fractal analysis of scale invariance. Engineering Fracture Mechanics, 68, 1975-2012.

Tyler, S.W. & Wheatcraft, S.W. (1989). Application of fractal mathematics to soil water retention estimation. Soil. Sci. Soc. Am. J., 53, 987-996.

Wendt, M. & Balusu, R. (2002). CFD modeling of longwall goaf gas flow dynamics. Coal and Safety 20, 17-34.

Wheatcraft, S.W. & Tyler, S.W. (1988). An explanation to scale-dependent dispersivity in heterogeneous aquifers using concepts of fractal geometry. Water Res. Research, 24, 566-578.

Whittles, D.N., Lowndes, I.S., Kingman, S.W., Yates, C., & Jobling, S. (2006). Influence of geotechnical factors on gas flow experienced in a UK longwall coal mine panel. International Journal of Rock Mechanics and Mining Sciences 43, 369-387.

Yavuz, H. (2004). An estimation of cover pressure re-establishment distance and pressure distribution in the goaf longwall coal mines. International J. of Rock Mech. and Mining Sciences 41, 193-205.

Yu, B.M. & Cheng, P. (2002). A fractal model for bi-dispersed porous media. Int. J. of Heat and Mass Transfer, 45 (11), 2983-2993.

Yu, B.M. & Liu, W. (2004). Fractal analysis of permeabilities for porous media. AIChE Journal 50(1), 46-57.

Yuan, L. & Smith, A.C., (2008). Effects of ventilation and gob characteristics on spontaneous heating in longwall gob areas. Proc. 12th U.S./North American Mine Ventilation Symposium, pp. 141-147, Reno, NV, June 9-11.